Electroless Plating of Iron onto Cellulose Fibers

Michael A. Dinderman,† Walter J. Dressick,† Cynthia N. Kostelansky,† Ronald R. Price,† Syed B. Qadri,‡ and Paul E. Schoen*,†

Center for Biomolecular Science and Engineering (Code 6900) and Materials Science and Technology Division (Code 6364), Naval Research Laboratory, 4555 Overlook Avenue SW, Washington, D.C. 20375

Received March 17, 2006. Revised Manuscript Received June 28, 2006

We describe a new electroless iron bath capable of depositing a ferromagnetic FeB coating onto Pd/Sn-catalyzed substrates at room temperature without the need for an accompanying galvanic couple and illustrate its use for the fabrication of magnetic cellulose microfibers. The new electroless iron bath contains Fe^{2+} as the metal source, citrate as the metal chelator, boric acid buffer as the pH controller, and borohydride as the reductant. Surface analysis following plating confirms the deposition of an amorphous FeB coating of composition $\sim Fe_{10}B$ onto the microfiber surface. Through the use of two-level factorial design statistical methods, we characterize the effects of plating variables (i.e., bath pH and concentrations of each bath component) on bath behavior, identifying pH as the sole factor influencing the mass of plated Fe and establishing optimal, reproducible conditions for electroless Fe deposition.

Introduction

Electroless metallization is a method for the deposition of a metal film onto a substrate via catalyzed chemical reduction of solution-phase metal ions at the substrate surface.[1−3] A typical electroless plating bath comprises an aqueous solution containing metal ions (i.e., metal source) bound by complexation with a ligand chelator, a buffer to control pH, and a reductant. Often, stabilizers, refining agents, and other minor components are added to the plating bath to improve the lifetime of the bath and the quality of the plated metal.[2,3] Upon contact of the plating bath with an appropriate catalytic surface, separate redox reactions involving reduction of metal ions to metal and oxidation of the reducing agent occur to plate metal onto the substrate surface. Specific plating bath conditions (e.g., pH and metal ion, reductant, and chelator types and concentrations), as governed by mixed potential theory,[3] are necessary to initiate and sustain electroless plating. Further conditions (e.g., bath stability and a controlled deposition rate) must be met to selectively plate a metal layer of the desired physical, electronic, or magnetic properties onto a substrate.

Electroless plating has been studied both academically and industrially for decades. Many electroless plating baths have been developed to deposit commercially desirable metals (i.e., cobalt, copper, gold, nickel, platinum, and silver) onto a variety of substrates. For example, bulk-scale commercial plating baths are available for the electroless plating of copper and nickel alloys (e.g., NiP and NiB).[1,2] As a result, the electroless plating method is used widely in industry for aerospace, automotive, and electronics applications.[1] For example, in our laboratory we have recently developed methods for the fabrication of micro- and nanoscale patterned electroless metal films useful as plasma-resistant etch masks and electrically conductive pathways in electronic circuit manufacture.[4]

Recently, there has been an interest in developing methods for the electroless deposition of novel magnetic materials[5−19] (e.g., iron-plated particles) because of their expected utility

* To whom correspondence should be addressed. E-mail: pschoen@cbmse.nrl.navy.mil.

† Center for Biomolecular Science and Engineering.

‡ Materials Science and Technology Division.

(1) Mallory, G. O.; Hajdu, J. B. *Electroless Plating: Fundamentals and Applications*; American Electroplaters and Surface Finishers Society: Orlando, FL, 1990; Chapter 1.
(2) Ohno, I. *Mater. Sci. Eng.* **1991**, *A146*, 33.
(3) Lin, Y.-M.; Yen, S.-C. *Appl. Surf. Sci.* **2001**, *178*, 116.
(4) (a) Chen, M.-S.; Brandow, S. L.; Dressick, W. J. *Thin Solid Films* **2000**, *379*, 203. (b) Chen, M.-S.; Dulcey, C. S.; Brandow, S. L.; Leonard, D. N.; Dressick, W. J.; Calvert, J. M.; Sims, C. W. *J. Electrochem. Soc.* **2000**, *147*, 2607. (c) Ma, D. I.; Shirey, L.; McCarthy, D.; Thompson, A.; Qadri, S. B.; Dressick, W. J.; Chen, M.-S.; Calvert, J. M.; Kapur, R.; Brandow, S. L. *Chem. Mater.* **2002**, *14*, 4586. (d) Dobisz, E. A.; Bass, R.; Brandow, S. L.; Chen, M.-S.; Dressick, W. J. *Appl. Phys. Lett.* **2004**, *82*, 478. (e) Chen, M.-S.; Brandow, S. L.; Schull, T. L.; Chrisey, D. B.; Dressick, W. J. *Adv. Funct. Mater.* **2005**, *15*, 1364. (f) Chen, M.-S.; Dulcey, C. S.; Chrisey, L. A.; Dressick, W. J. *Adv. Funct. Mater.* **2006**, *16*, 774.
(5) Wang, L.; Zhao, L.; Zhang, B.; Hu, W.; Shu, X.; Sheng, X.; Fang, Z. *J. Alloys Compd.* **1999**, *287*, 234.
(6) Wang, L.; Zhang, B.; Yi, G.; Ouyang, Y.; Hu, W. *J. Alloys Compd.* **1997**, *255*, 231.
(7) Hu, W.; Zhang, B. *Trans. Inst. Met. Finish.* **1993**, *71*, 30.
(8) Fujita, N.; Tanaka, A.; Makino, E.; Squire, P.; Lim, P.; Inoue, M.; Fujii, T. *Appl. Surf. Sci.* **1997**, *113/114*, 61.
(9) Ruscior, C.; Croiala, E. *J. Electrochem. Soc.* **1971**, *118*, 696.
(10) Drovosekov, A. B.; Ivanov, M. V.; Lubnin, E. N. *Prot. Met.* **2004**, *40*, 89.
(11) Fujita, N.; Inoue, M.; Arai, K.; Lim, P.; Fujii, T. *J. Appl. Phys.* **1998**, *83*, 7294.
(12) Wang, L.; Zhao, L.; Huang, G.; Yuan, X.; Zhang, B.; Zhang, J. *Surf. Coat. Technol.* **2000**, *126*, 272.
(13) Yokoshima, T.; Kaneko, D.; Akahori, M.; Nam, H.-S.; Osaka, T. *J. Electroanal. Chem.* **2000**, *491*, 197.
(14) Wang, S.-L. *Surf. Coat. Technol.* **2004**, *186*, 372.
(15) Kim, S.-S.; Kim, S.-T.; Ahn, J.-M.; Kim, K.-H. *J. Magn. Magn. Mater.* **2004**, *271*, 39.
(16) Krebs, J. J.; Rubinstein, M.; Lubitz, P.; Harford, M. Z.; Baral, S.; Shashidar, R.; Ho, R. S.; Chow, G. M.; Qadri, S. *J. Appl. Phys.* **1991**, *70*, 6404.
(17) Yang, Y.; Zhang, B.; Xu, W.; Shi, Y.; Jiang, Z.; Zhou, N.; Gu, B.; Lu, H. *J. Magn. Magn. Mater.* **2003**, *256*, 129.

10.1021/cm060649o CCC: $33.50 © 2006 American Chemical Society
Published on Web 08/09/2006

in various electronics applications.[11,17−23] Consequently, a variety of methods have been described for electroless deposition of iron-based ferromagnetic materials, together with the physical and magnetic properties of the resulting deposits.[5−18] However, several of these methods require a sacrificial galvanic couple[5−9] (e.g., an Al strip in contact with the electroless bath and metallic substrate to be plated), limiting their usefulness to macroscopic substrates. In addition, all the methods require elevated temperatures to achieve successful plating. The resulting deposits are invariably composed of an iron alloy (e.g., FeB, FeP, FeCo, FeNi, FeSnB, FeMoB, or FeNiP),[5−15] and the composition of each deposit is dependent on the bath formulation and plating conditions employed. Generally, the resulting deposits are amorphous but show improved crystallinity after being annealed. Although numerous macroscale substrates (e.g., copper sheets, copper foils, carbon steel foils, and Cu/Cr-coated glass) have been plated, fewer examples exist of metallized microscale substrates, which exhibit useful dielectric and magnetic properties when incorporated into composite matrixes.[15,18]

Tubular microstructures, derived from natural systems, represent a common biological motif that has been readily exploited for various applications of technological interest.[24] For example, in our laboratory we have shown that an electroless plating method may be utilized to coat hollow phospholipid[25] and halloysite[26] microtubules with Ni or Cu. The resulting metallized microtubules were shown effective as containers for microencapsulation and controlled release of chemical agents,[27] tested as field emitters for electronic display applications,[28] and studied for use in dielectric applications.[11,29,30] Recently, we have shown that lipid microtubules can function as effective templates for the fabrication of nanoscale Cu helical structures via the selective electroless metallization of the tubule surface seams.[31] Although lipid microtubules possess many desirable properties (e.g., high aspect ratio, hollow center, and accessible interior and exterior surfaces easily metallized by electroless plating), they are also fragile. Lipid microtubules are readily broken into shorter fibers during standard manipulations associated with their metallization (e.g., binding Pd/Sn electroless catalysts to the surface and washing procedures). In addition, lipid tubule templates are easily destroyed by melting at the elevated temperatures utilized by many electroless baths, including known Fe baths,[5−15] to enhance metal deposition. The temperature sensitivity of tubules therefore requires formulation and use of less efficient baths operating near room temperature. To overcome these issues, we have begun to investigate other more robust natural products, such as cellulose fibers, having desirable structural features similar to those of lipid tubules, as metallization templates.

Recently, we described a new process for the successful plating of cellulose fiber templates catalyzed by a commercial Pd/Sn electroless catalyst using electroless copper.[32] In this paper, we describe a new electroless iron bath capable of depositing a ferromagnetic FeB coating onto Pd/Sn-catalyzed substrates at room temperature without the need for an accompanying galvanic couple. We illustrate its use for the fabrication of magnetic cellulose microfibers. The new electroless iron bath is comprised of Fe^{2+} as the metal source, citrate as the metal chelator, boric acid buffer as the pH controller, and borohydride as the reductant. Surface analysis following plating confirms the deposition of an amorphous FeB coating onto the surface of Pd/Sn-catalyzed cellulose microfibers. Through the use of a two-level factorial design statistical method,[33] we characterize the effects of plating variables (i.e., bath pH and concentrations of each bath component) on bath behavior and identify optimal reproducible conditions for electroless Fe deposition. Detailed investigations of the magnetic properties of the plated fibers are currently under way[34] and will be reported in a future publication elsewhere.

Experimental Section

Materials. All materials were ACS reagent grade or equivalent and were used as received. Fibrous cellulose (medium length, ~20

(18) Behroozi, F.; Orman, M.; Reese, R.; Stockton, W.; Calvert, J.; Rachford, F.; Schoen, P. *J. Appl. Phys.* **1990**, *68*, 3688.
(19) Shacham-Diamand, Y.; Sverdlov, Y. *Microelectron. Eng.* **2000**, *50*, 525.
(20) Shin, J. Y.; Oh, J. H. *IEEE Trans. Magn.* **1993**, *29*, 3437.
(21) Matsumoto, M.; Miyata, Y. *IEEE Trans. Magn.* **1997**, *33*, 4459.
(22) Wu, M.; Zhao, Z.; He, H.; Yao, X. *J. Magn. Magn. Mater.* **2000**, *217*, 89.
(23) Soloman, M. A.; Kurian, P.; Anantharaman, M. R.; Joy, P. A. *J. Appl. Polym. Sci.* **2003**, *89*, 769.
(24) Shimizu, T.; Masuda, M.; Minamikawa, H. *Chem. Rev.* **2005**, *105*, 1401.
(25) (a) Price, R. R.; Schnur, J. M.; Ratna, B. R.; Spector, M. U.S. Patent 6,936,215, Aug 30, 2005. (b) Price, R. R.; Schnur, J. M.; Schoen, P. E.; Zabetakis, D.; Spector, M. U.S. Patent 6,013,206, Jan 11, 2000. (c) Schnur, J. M.; Price, R.; Schoen, P.; Yager, P.; Calvert, J. M.; Georger, J.; Singh, A. *Thin Solid Films* **1987**, *152*, 181. (d) Zabetakis, D. *J. Mater. Res.* **2000**, *15*, 2368. (e) Zabetakis, D. U.S. Patent 6,913,828, July 5, 2005. (f) Spector, M.; Price, R.; Schnur, J. *Adv. Mater.* **1999**, *11*, 337.
(26) (a) Shchukin, D. G.; Sukhorukov, G. B.; Price, R. R.; Lvov, Y. M. *Small* **2005**, *1*, 510. (b) Baral, S.; Brandow, S.; Gaber, B. P. *Chem. Mater.* **1993**, *5*, 1227.
(27) (a) Price, R. R.; Eden, R. D.; Gaber, B. P. U.S. Patent 6,401,816, June 11, 2002. (b) Price, R. R.; Gaber, B. P.; Lvov, Y. *J. Microencapsulation* **2001**, *18*, 713. (c) Price, R. R.; Schnur, J. M.; Schoen, P. E.; Testoff, M.; Georger, J. H., Jr.; Rudolph, A.; Brady, R. F. U.S. Patent 6,280,759, Aug 28, 2001. (d) Price, R. R.; Schnur, J. M.; Rudolph, A. S.; Selinger, J.; Singh, A.; Gaber, B. P. U.S. Patent 5,705,191, Jan 6, 1998. (e) Price, R. R.; Gaber, B. P. U.S. Patent 5,651,976, July 29, 1997. (f) Price, R. R.; Schnur, J. M.; Schoen, P. E.; Testoff, M.; Georger, J. H., Jr.; Rudolph, A.; Brady, R. F. U.S. Patent 5,492,696, Feb 20, 1996. (g) Schnur, J. M.; Price, R.; Rudolph, A. S. *J. Controlled Release* **1994**, *28*, 3. (h) Price, R.; Patchan, M. *J. Microencapsulation* **1991**, *8*, 301.
(28) (a) Chow, G.-M.; Stockton, W. B.; Price, R.; Baral, S.; Ting, A. C.; Ratna, B. R.; Schoen, P. E.; Schnur, J. M.; Bergeron, G. L.; Czarnaski, M. A.; Hickman, J. J.; Kirkpatrick, D. A. *Mater. Sci. Eng., A* **1992**, *158*, 1. (b) Kirkpatrick, D. A.; Schnur, J. M.; Schoen, P. E.; Price, R. R.; Manheimer, W. M. U.S. Patent 5,089,742, Feb 18, 1992.
(29) Stockton, W.; Lodge, J.; Rachford, F.; Orman, M.; Falco, F.; Schoen, P. *J. Appl. Phys.* **1991**, *70*, 4679.
(30) Browning, S.; Lodge, J.; Price, R.; Schelleng, J.; Schoen, P.; Zabetakis, D. *J. Appl. Phys.* **1998**, *84*, 6109.
(31) Price, R. R.; Dressick, W. J.; Singh, A. *J. Am. Chem. Soc.* **2003**, *125*, 11259.
(32) Zabetakis, D.; Dinderman, M.; Schoen, P. *Adv. Mater.* **2005**, *17*, 734.
(33) (a) Box, G. E. P.; Hunter, W. G.; Hunter, J. S. *Statistics for Experimenters: An Introduction to Design, Data Analysis, and Model Building*; John Wiley & Sons: New York, 1978; Chapter 10. (b) Bayne, C. K.; Rubin, I. B. *Practical Experimental Designs and Optimization Methods for Chemists*; VCH Publishers: Deerfield Beach, FL, 1986; Chapter 4.
(34) Qadri, S. Work in progress.

μm diameter × ~200 μm length, $\rho_c = 0.6$ g·cm^{-3}), boric acid, sodium hydroxide (pellets), sodium citrate dihydrate (USP grade), and iron(II) sulfate heptahydrate were obtained from Sigma-Aldrich Corp. Cataprep 404 (sodium bisulfate) and Cataposit 44 (acidic tin chloride−palladium catalyst dispersion) were purchased from the Shipley Co. unit of Rohm and Haas (Marlborough, MA). Ethanol (200 proof, USP) was received from the Warner Graham Co. (Cockeysville, MD). Milli-Q water (18.2 MΩ·cm^{-1}) was generated in-house and was used in the preparation of all aqueous solutions and during all fiber washing processes. Nitrogen gas was obtained as boil-off from an in-house liquid nitrogen reservoir.

Fiber Catalysis. Catalysis of cellulose fibers was reported in a previous publication.[32] Briefly, Cataprep 404 (250 g, white solid) was first dissolved in water (2.5 L) in a glass beaker (4.0 L) with magnetic stirring at room temperature. Cellulose fibers (100 g, white solid) were added to the Cataprep 404 solution, which was stirred for 30 min to completely disperse the fibers. Cataposit 44 (50 mL, brown liquid) was then added, and the dispersion was stirred for an additional 60 min. The resulting Pd/Sn-catalyzed cellulose fibers (brown solid) were recovered by vacuum filtration, washed in water (2.0 L), and dried in a convection oven (6 h in air at 105 °C). The catalyzed fibers were stored in plastic bags under a nitrogen atmosphere at room temperature until needed for experiments. Catalyzed fibers prepared and stored in this manner maintained their activity for electroless metal deposition for at least 12 months.

Plating Bath Preparations. Each plating bath was comprised of Milli-Q water, source metal ion (iron(II) sulfate heptahydrate), metal chelator (sodium citrate dihydrate), pH stabilizer (boric acid buffer solution), and reducing agent (sodium borohydride). Compositions of each plating bath were governed by the two-level factorial designs[33] used to study and map the effects of plating variables on the bath performance, as described below. Separate stock solutions containing appropriate metal/chelator ratios and pH buffers required for each two-level factorial design were prepared within 24 h of use and combined as described below to improve consistency and facilitate bath preparations. To prepare the metal/chelator stock solutions, appropriate weighed quantities of ferrous sulfate heptahydrate and sodium citrate dehydrate were placed in a 2.5 L beaker and dissolved in ~1.8 L of water with stirring. The solution and aqueous washings were transferred into a 2.50 L volumetric flask and diluted to the mark with water. The stock pH buffers, containing a constant 0.500 M total borate concentration, were prepared by dissolving 77.29 g (1.250 mol) of boric acid and a quantity of NaOH pellets calculated to give the desired final pH in ~2.2 L of water with stirring in a 2.5 L beaker. When the solids were dissolved and the solution had cooled to room temperature, the pH was measured using a pH meter. If necessary, the solution was titrated with additional ~1.2 M NaOH(aq) solution to adjust the final pH. The solution and aqueous washings were then transferred to a 2.50 L volumetric flask and diluted to the mark with water. The various required metal/chelator and pH buffer stock solutions were transferred to separate polypropylene containers that were tightly sealed for storage until the solutions were needed for plating experiments.

Each plating bath was prepared by addition of the appropriate stock buffer solution (250 mL) to the proper stock metal/chelator solution (250 mL) contained in a plastic beaker (1 L) at room temperature (22 ± 2 °C) to achieve a plating bath with the variable values designated by the factorial design. The pH of the resulting solution was measured, the beaker was placed in a fume hood, and the appropriate quantity of solid sodium borohydride was added within 10 min and dissolved with vigorous manual stirring to complete the preparation of the electroless Fe bath.

Fiber Metallization and Recovery. For each experiment a 250 mg sample of Pd/Sn-catalyzed cellulose fibers was quickly added in one portion with manual stirring to the Fe electroless bath (as soon as the sodium borohydride had dissolved) to initiate Fe deposition. The bath was manually stirred for 30 s, every 10 min, for the required time duration of the experiment. For experiments requiring 24 h plating times, samples were stirred for the first 4 h and then left unstirred. After the required amount of plating time had passed, a magnet placed under the beaker was utilized to separate the fibers from the liquid phase. The plated fibers were washed with water (3 × 100 mL) and separated using the magnet again until the washings were colorless. They were then washed with ethanol (1 × 100 mL), separated using the magnet, redispersed in fresh ethanol (~100 mL), carefully decanted into a 250 mL filter funnel containing a preweighed piece of filter paper (Fisherbrand Q5 quantitative ashless) prewetted with ethanol, and recovered by vacuum filtration. The plated fibers were carefully washed on the filter successively with ethanol (2 × 100 mL) and acetone (2 × 100 mL) and air suction dried for ~30 s following the last acetone wash. The filter paper containing the plated fibers was removed from the funnel and transferred to a preweighed plastic jar, which was placed in a heated vacuum oven (N_2 atmosphere, 40 °C) overnight to complete drying. The jars containing the plated fibers and filter papers were then stored under a nitrogen atmosphere at room temperature until the plated fibers and filter papers were needed for analysis.

Fiber Characterization and Instrumentation. From each experiment, the mass of the plated fibers, if any, was recorded and used to determine the amount of Fe deposited after subtraction of the initial mass of cellulose used (i.e., 0.250 g). A minimum of 200 fibers from each sample was then observed under a Leitz-Wetzlar optical microscope (20× magnification) and photographed to determine the average quality (i.e., percentage of the fibers plated and morphology of the metal deposit) of the plated surface. Plating of the surface of an individual fiber, when it occurred, was essentially complete (99 ± 2%). Therefore, fibers appeared either translucent brown (catalyzed, unplated) or solid black (plated), and the plating percentage was determined by calculating the fraction of fibers that appeared black. Dried, plated fibers were determined to be ferromagnetic on the basis of whether they were attracted to a bulk magnet.

Additionally, sample 8 from the optimized design matrix II was randomly selected and characterized further to determine the composition and morphology of the metal deposit. For this sample, elemental analyses via instrumental neutron activation analysis (Fe, Sn, and Pd) and prompt γ neutron activation analysis (Boron) were provided by Elemental Analysis, Inc. (Lexington, KY). A Rigaku ATX advanced thin film X-ray diffractometer system (Cu Kα radiation from an 18 kW rotating anode source) was used to acquire the X-ray diffraction (XRD) data; the plated microfiber samples were mounted on a single Si(001) crystal to minimize background scattering.[35] XPS spectra were acquired using a Thermo VG Scientific Escalab 220i-XL with a monochromatic Al Kα source, a hemispherical electron analyzer, and a magnetic electron lens. The sample was prepared immediately before use by depositing ~25 mg of plated fibers onto a conducting carbon adhesive tab (Electron Microscopy Sciences, no. 77825-12) affixed to a 2 cm × 2 cm Cu foil that had previously been cleaned by successive 5 min sonications in ethanol and acetone. Measurements were performed with a base pressure of 1 × 10^{-9} Torr at room temperature. Survey scans were acquired in the 0−1400 eV binding energy range (100 eV pass energy). High-resolution normal-

(35) Cullity, B. D. *Elements of X-Ray Diffraction*; Addison-Wesley: Reading, MA, 1978; p 284.

emission angle-integrated scans of the C(1s) and B(1s) regions were acquired with 15−20 eV windows (20 eV pass energy). The XPS signals were calibrated to the C(1s) peak at 284.6 eV. The high-resolution spectra were fit using Universal Spectrum Processing and Analysis Program for ESCA-Spectra (version 2005) software.

Statistical Analyses. Two-level 2^n-factorial design methods,[33] where n is the number of variables studied, were used to quantitatively estimate the effects of each variable and interaction of variables on the experimental responses as described in detail in the Supporting Information. Briefly, the variables studied included various combinations of the pH, [Fe(II)], [citrate], and [BH_4^-] as described in the text below for each design. Each variable to be studied was assigned a low and high value, coded as −1 and +1, respectively, in each design. Levels of the citrate and borohydride variables were defined as mole ratios relative to the [Fe(II)] variable, as specifically identified later in the text. Consequently, each design comprised a 2^n row × n column matrix, in which each column is associated with a specific variable and each row defines a specific experiment, containing entries of −1 or +1 signifying the coded level of each variable in that experiment. Each design matrix was set up in standard order, such that the nth column consisted of 2^{n-1} entries of −1 followed by 2^{n-1} entries of +1, in alternating fashion to facilitate data analysis.

Each experiment was performed by randomly selecting a row of the design matrix and reading the code (i.e., −1 or +1) associated with each column entry corresponding to a particular variable for that row. An electroless bath was then prepared containing the appropriate level of each variable designated by the codes and used to plate the catalyzed cellulose fibers. The mass of Fe plated (R_1) and the percentage of fibers plated (R_2) were measured as separate experimental responses and associated with that row of the matrix. The process was repeated for another randomly chosen row (i.e., experiment) until all 2^n design experiments were completed to generate response columns for the design matrix. Experiments associated with the final bath optimization described in matrix II were repeated twice to ensure reproducibility of the results.

Yates' algorithm was used to compute the effects, $E(R)_i$ ($i = 1, 2, ..., 2^n$), of each variable or interaction of variables on a given response, R. $E(R)_i$ calculations were checked using the sum of squares method.[33] The calculated $E(R)_i$ were identified with the variable or combination of variables having the +1 designation(s) in the ith row of the design matrix, then arranged in increasing order from most negative to most positive, and serially assigned a cumulative probability, P_i, using eq 1. A normal probability plot

$$P_i = 100(i - 1/2)/(2^n - 1)\ (i = 1, 2, ..., 2^n - 1) \qquad (1)$$

of each $E(R)_i$ (abscissa) vs its associated P_i value (ordinate) gave a straight line symmetrical about the abscissa zero containing points corresponding to variables and interactions of variables having no significant influence on the response. Points associated with variables or interactions of variables exhibiting a real influence on the experimental response were identified by deviations from this straight line at the positive and/or negative extrema. A specific example is shown in Figure 4A. For normal probability plots in which significant effects were identified, residuals $\Delta(R)_i$ were calculated using a reverse Yates algorithm as a further diagnostic check. The residuals were ordered from most negative to most positive, and each was assigned a cumulative probability, P_i, according to eq 2. Plots of $\Delta(R)_i$ (abscissa) vs P_i (ordinate) on

$$P_i = 100(i - 1/2)/(2^n)\ (i = 1, 2, ..., 2^n) \qquad (2)$$

normal probability paper yielded straight lines containing all points in all cases, consistent with the correct identification of the significant effects in the normal probability plot for the corresponding effects.

Results and Discussion

Because of its less favorable redox and catalytic activities compared to more noble metals, Fe is often electrolessly co-deposited in the form of alloys with other more active metals, such as Ni or Co.[12−15] Electroless baths for the deposition of binary alloys containing only Fe, together with smaller amounts of nonmetals such as B or P,[7−11] are less common, but provide a convenient starting point for the development of new Fe electroless baths due to their comparative simplicity and low cost. Such baths typically contain a ferrous salt complexed by a carboxylate-based chelator ligand such as citrate, tartrate, or glycine as the metal source, in combination with a strong reducing agent such as borohydride or hypophosphite in alkaline solution. Solution pH in these baths is typically adjusted by direct addition of base and often moderated only by the buffer capacity of any free ligand present. Therefore, we opted to initiate our investigation using baths prepared from ferrous sulfate, sodium citrate, and sodium borohydride in an alkaline borate buffer ($pK_{a1} = 9.23$) solution to minimize potential pH variations during plating due to metal ion−buffer interactions and changes in free ligand concentrations.

To most efficiently identify and assess the effects due to changes in levels of bath component variables on the amount and quality of plated material and optimize our process, we employed two-level factorial statistical design methods[33] to plan, execute, and analyze our experiments. As our starting point, we used the 2^4-factorial design matrix I shown in Figure 1 (top) to screen the effects of the [Fe(II)], [citrate], [BH_4^-], and pH variables on the completeness and quantity of plating and refine the range of each variable, on the basis of the observed plating trends, for subsequent studies. For each variable, minimum and maximum values, coded respectively by entries of −1 and +1 in Figure 1 (top), were chosen to cover what we believed to be the widest range capable of providing a stable plating bath and producing magnetic fibers, on the basis of literature precedents[5−15] and our previous experience with electroless bath formulations. For bath alkalinity, we selected a range of 1 pH unit with minimum and maximum levels of pH 9.2 (−1) and pH 10.2 (+1), respectively, controlled by the borate buffer. Initial levels for [Fe(II)] were 0.005 M (−1) and 0.050 M (+1). The [citrate] and [BH_4^-] ranges were defined on the basis of the [Fe(II)] values. The lower [citrate] level (−1) was set at 3[Fe(II)], an amount just sufficient for complete formation of a tris-bidentate citrate complex of Fe(II) in solution, with the high level at 5[Fe(II)] providing baths containing excess citrate ligand. Because noticeable hydrogen gas evolution consistent with [BH_4^-] decomposition occurred during use of the baths, [BH_4^-] levels of [Fe(II)] (−1) and 5[Fe(II)] (+1) were chosen to ensure that sufficient reductant remained available for reduction of Fe(II) during the course of each experiment. Other parameters, including the bath volume (500 mL), quantity of catalyzed cellulose (250 mg), and temperature (22 ± 2 °C) remained constant during the fixed 24 h plating time.

Sample	[Fe(II)]	[Citrate]	[BH_4^-]	pH
1	–1	–1	–1	–1
2	+1	–1	–1	–1
3	–1	+1	–1	–1
4	+1	+1	–1	–1
5	–1	–1	+1	–1
6	+1	–1	+1	–1
7	–1	+1	+1	–1
8	+1	+1	+1	–1
9	–1	–1	–1	+1
10	+1	–1	–1	+1
11	–1	+1	–1	+1
12	+1	+1	–1	+1
13	–1	–1	+1	+1
14	+1	–1	+1	+1
15	–1	+1	+1	+1
16	+1	+1	+1	+1

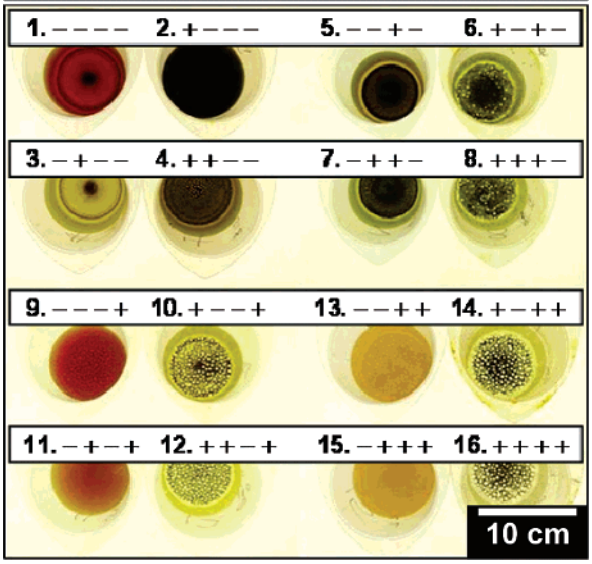

Figure 1. 2^4-factorial design matrix I. (Top) Design matrix showing the Fe(II), citrate, and borohydride concentration and pH variables with low and high coded levels designated as −1 and +1 table entries, respectively. Specific concentrations corresponding to the −1 and +1 designations for each variable are described in the text. (Bottom) Photograph showing the baths from the matrix experiments (top) after a 24 h plating time prior to isolation of the treated fibers. Other plating conditions are defined by the matrix (top) and described in the text. The identifier above each beaker serially lists the experiment number and the coded levels of Fe(II), citrate, and borohydride concentrations and pH, respectively, from the matrix (top). Note that we have used + and − rather than +1 and −1, respectively, for the beaker variable codes due to space limitations.

The photograph in Figure 1 (bottom) shows the baths containing the treated microfibers immediately after completion of the 24 h plating for each of the 16 experiments of the 2^4-factorial design matrix I. All plating baths were a clear, yellow-green color when first prepared, just prior to addition of the catalyzed cellulose fibers. Hydrogen gas evolution initiated upon addition of the fibers and metallization, when it occurred (vide infra), was evident within ∼5 min by blackening of the fibers. Plating was accompanied by bleaching of the bath color, yielding a frothy gray mixture. As plating rates and frothing decreased with time, new solution colors developed as shown in Figure 1 (bottom). In all cases, bath alkalinity increased only slightly (i.e., ∼0.1−0.2 pH unit) after plating, consistent with good control of the solution pH by the borate buffer.

Unfortunately, the deposition of gray-black, adherent, metal coatings onto the fibers in some experiments was accompanied or supplanted by other competitive processes in the baths, complicating interpretation of the results. For example, rapid color bleaching, plating, and gas evolution rates were observed for baths 6, 8, and (especially) 14 and 16, resulting in less adherent metal deposits which were partially separated from the fibers by means of the foaming action of the bath and/or mechanical manipulations during filtration. In contrast, baths 9, 11, 13, and 15 developed an orange-yellow color and cloudy appearance (see Figure 1 (bottom)), indicative of the formation of colloidal iron hydroxide/oxide (i.e., rust), within ∼90 min after initiation of plating. Recovered fibers from baths 9 and 11 were orange-brown in color and nonmagnetic, consistent with the deposition of rust, rather than metal, onto the fibers. Gray-black, magnetic metal fibers were successfully isolated from baths 13 and 15, though the fibers from bath 15 were visibly contaminated with particles of the orange-brown rust precipitate. Although solution color changes in baths 1−4 generally differed from those of baths 9, 11, 13, and 15, these baths also yielded brown, nonmagnetic fibers (e.g., see sample 3, Figure 1 (bottom)) that were difficult to recover during filtration.

Although these problems preclude a quantitative statistical analysis of the effects of the variables on the completeness and amount of plating, design matrix I nevertheless yields sufficient qualitative information to narrow the range of variables to improve the plating behavior. For example, examination of matrix I indicates that the formation of nonmagnetic fibers corresponds to low [BH_4^-] levels, generally in combination with low pH and/or low [Fe(II)] levels, in baths 1−4, 9, and 11. Likewise, formation and precipitation of rust in baths 9, 11, 13, and 15 is qualitatively correlated with low [Fe(II)] and high pH levels in these baths. In addition, the design results suggest that poor adhesion of the metal deposit to the fibers is likely associated with high [Fe(II)] and [BH_4^-] levels in baths 6, 8, 14, and 16.

Using these qualitative observations, we set up a second design matrix in which the ranges of the variables were adjusted to address these problems. For this second matrix, the high levels (+1) for [Fe(II)] (i.e., 0.05 M) and pH (i.e., 10.2) remained unchanged, but the low levels (−1) were raised to [Fe(II)] = 0.025 M and pH 9.7 to minimize the formation of nonplated fibers. Because visual observations from the matrix I experiments suggested that metal deposition

Table 1. Bath Optimization, a 2^3-Factorial Design Matrix, Arranged in Standard (Yates') Order

sample no.	[Fe(II)],[a,b] F[c]	[BH_4^-],[a,b] B[c]	pH,[b] H[c]	Fe mass (g) measured, $(R_1)_i$[d]	Fe mass (g) effect, $E(R_1)_i$[e]	Fe mass (g) residual, $\Delta(R_1)_i$[f]	Fe % plating measured, $(R_2)_i$[g]	Fe % plating effect, $E(R_2)_i$[h]
1	−1	−1	−1	0.201	0.184	0.008	99.11	99.437
2	+1	−1	−1	0.225	0.008	−0.051	100.00	0.589
3	−1	+1	−1	0.243	−0.018	0.019	99.51	0.398
4	+1	+1	−1	0.198	−0.001	0.025	100.00	−0.411
5	−1	−1	+1	0.176	−0.0655	−0.019	98.37	−0.435
6	+1	−1	+1	0.170	0.0185	0.026	99.48	−0.101
7	−1	+1	+1	0.100	−0.0255	0.008	99.58	0.195
8	+1	+1	+1	0.159	0.0335	−0.016	99.45	−0.208

[a] Concentration (mol·L^{-1}) of the component in the plating bath. [b] The +1 and −1 symbols signify the high and low levels of each variable, respectively, used for each experiment, as described and defined in the text. (See also the Experimental Section and Supporting Information for additional details.) [c] Identifier label for each variable, as used in statistical analyses and Figure 4. [d] Mass of plated Fe, in units of grams, after the initial mass (0.250 g, catalyzed cellulose fibers) was subtracted from the final mass (Fe-plated, cellulose fibers) for each sample. Uncertainty ±15%. [e] Estimates of factor effects and interactions, calculated from the forward Yates algorithm matrix for mass of plated Fe data (see Table S1). [f] Residual values, calculated from the reverse Yates algorithm analysis matrix for mass of plated Fe data (see Table S2). [g] Percentage of recovered fibers that appeared black (i.e., Fe-plated) when viewed under an optical microscope at 20× magnification. Uncertainty ±1%. [h] Estimated effects, calculated from the forward Yates algorithm matrix for percentage of Fe-plated fibers data (see Table S3).

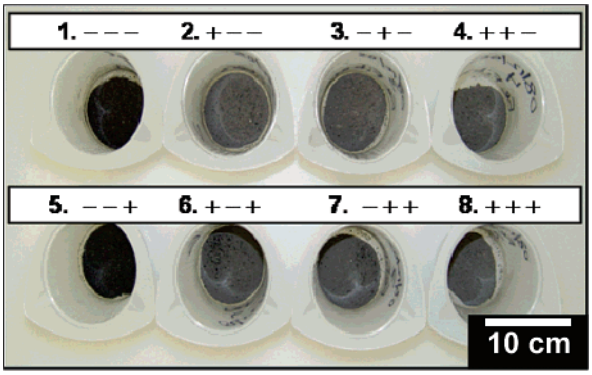

Figure 2. Plating results from 2^3-factorial design matrix II. Each numbered beaker shows the dried, metal-plated fibers obtained from the corresponding matrix II experiment and coded Fe(II) and borohydride concentration and pH levels summarized in Table 1. Note that we have used + and − rather than +1 and −1, respectively, for the beaker variable codes due to space limitations.

was essentially complete (i.e., >∼95%) after 4−5 h,[36] plating time was also reduced from 24 to 4 h to limit the possibility for competitive precipitation of iron hydroxide/oxide. In addition, to lower the activity of the baths and improve the adhesion of the plated metal, we reduced the high level (+1) for [BH_4^-] to 2[Fe(II)], keeping the low level (−1) unchanged at [Fe(II)]. Finally, because [citrate] was not identified as an important factor affecting plating in our qualitative analysis of matrix I, it was fixed at a constant level of 5[Fe(II)] for all experiments in matrix II. Consequently, matrix II comprised a 2^3-factorial design shown in Table 1 in which the three variables examined were [Fe(II)], [BH_4^-], and pH.

Plated fiber results from the eight experiments associated with matrix II are shown in the photograph of Figure 2. In contrast to matrix I, the problems associated with iron hydroxide/oxide precipitation, plating failure, and metal adhesion were completely eliminated by the changes in variable levels in matrix II. For all experiments, bath solutions remained pale yellow in color at the conclusion of the plating process and adherent, gray-black magnetic fibers shown in Figure 2 were isolated. As shown in the optical micrograph of Figure 3, the samples were predominantly comprised of completely plated, gray-black fibers (>∼98%). The samples were relatively free of debris (e.g., plated, nonfiber material), consistent with initiation and subsequent growth of metal on the catalyzed fiber surface as the primary metal deposition mechanism in our systems. Although

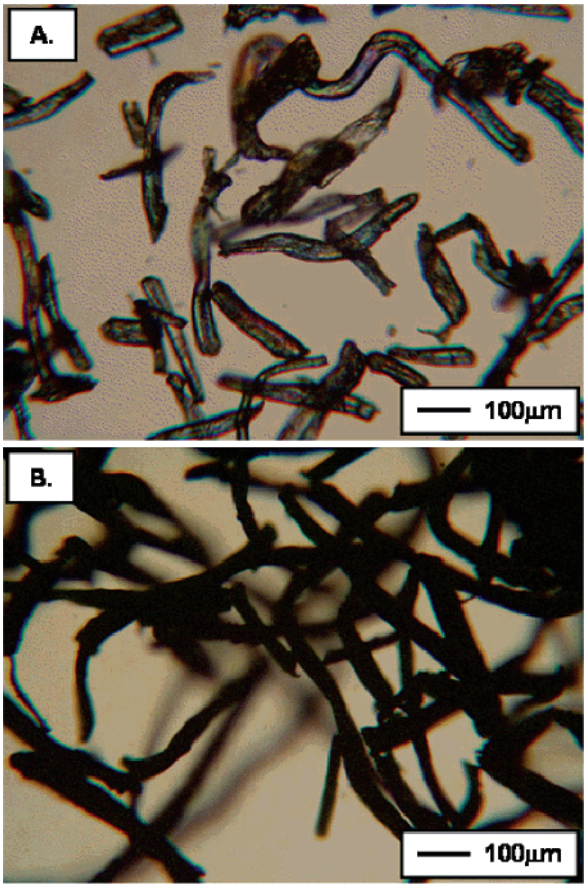

Figure 3. Optical micrographs (20×) of cellulose fibers: (A) catalyzed, unplated fibers, (B) dried, plated fibers from experiment 8 of matrix II. The variable levels are [Fe^{II}] = 0.05 M, [BH_4^-] = 0.10 M, [citrate] = 0.25 M, and pH 10.2.

(36) We confirmed that a 4 h plating time provided optimal metal deposition by repeating the experiments of matrix II using different plating times. For a 3 h plating time, metallization was variable and incomplete for several baths. The presence of unplated fibers, together with increased levels of plating debris, suggested that the thinner metal plate had delaminated from the fibers during filtration. Baths tested for longer times (e.g., 12−16 h) also yielded unplated fibers and additional metal debris. Subsequent observations suggested that this behavior was associated with corrosion of the metal plate in the alkaline citrate bath following decomposition of the borohydride.

surface features consistent with limited nonhomogeneous plating (e.g., nodules, pits) were occasionally observed, the level of such defective fibers never exceeded 5% of the fibers examined for a given experiment.

Unfortunately, attempts to use SEM or TEM to directly assess plating thickness and homogeneity via cross-sectional measurements of microtome samples containing epoxy-embedded plated fibers were confounded by image distortions due to the fibers' magnetic fields. However, the relative uniformity of the coating observed in the optical micrograph of Figure 3B permitted an estimate of plating thickness from the mass of plated Fe and the cylindrical fiber geometry. Specifically, for an experiment in which the mass of the cellulose fibers was exactly doubled as a result of Fe deposition, the average thickness of an Fe plate, y, uniformly covering a single cylindrical cellulose fiber could be estimated as $y \cong 3.56 \times 10^{-5}$ cm (i.e., 356 nm) from the positive root of eq 3. The terms r and h in eq 3 are the radius

$$2\pi y^3 + \pi(4r + h)y^2 + 2\pi r(r + h)y - \pi r^2 h\rho_c/\rho_{Fe} = 0 \quad (3)$$

and length (cm), respectively, of a cellulose fiber, ρ_c (= 0.6 g·cm^{-3}) is the density of the cellulose fibers, and ρ_{Fe} (= 7.86 g·cm^{-3}) is the density of Fe. For fibers less well plated, the Fe thickness calculated using the mass data (R_1) from matrix II in Table 1 scales according to eq 4. Using the data

$$y = (\text{mass of Fe (g)}/0.250\text{ g}) \times 356\text{ nm} \quad (4)$$

from Table 1, thickness estimates range from ~140 nm for the least plated sample from experiment 7 to ~346 nm for the most plated sample from experiment 3.

In addition to the measured masses of plated metal (R_1), Table 1 also summarizes the percentages of metal plated fibers (R_2) obtained as responses for each experiment. The effects (i.e., $E(R_1)$ and $E(R_2)$) for each response and residuals for the plated metal mass response (i.e., $\Delta(R_1)$), calculated using Yates' algorithm methods as described in the Experimental Section, are also separately tabulated. Details of these calculations are presented in Supporting Information Tables S1−S3. In addition, the variable or combination of variables associated with each $E(R_1)$ and $E(R_2)$ is identified by code letter(s), with F ≡ [Fe(II)], B ≡ [BH_4^-], and H ≡ pH, in the last column of Table 1.

The statistical analyses of the effects of the variables on the plating mass (R_1) and percentage plating (R_2) are shown by the normal probability plots in parts A and B, respectively, of Figure 4. In Figure 4A, only the point corresponding to the pH variable (≡H) deviates from the straight line defined by the other variables and their various combinations. Consequently, only the pH effect influences the quantity of metal plated, with the modest negative deviation signifying somewhat increased amounts of deposited metal associated with the use of lower pH baths. A plot of the residuals, shown as Figure S1 in the Supporting Information, forms a straight line through the abscissa zero, verifying that all effects other than pH are associated with random noise and are unimportant in determining the amount of metal plated. In contrast, all the effects in the normal probability plot of Figure 4B form a straight line with no deviations, indicating that the

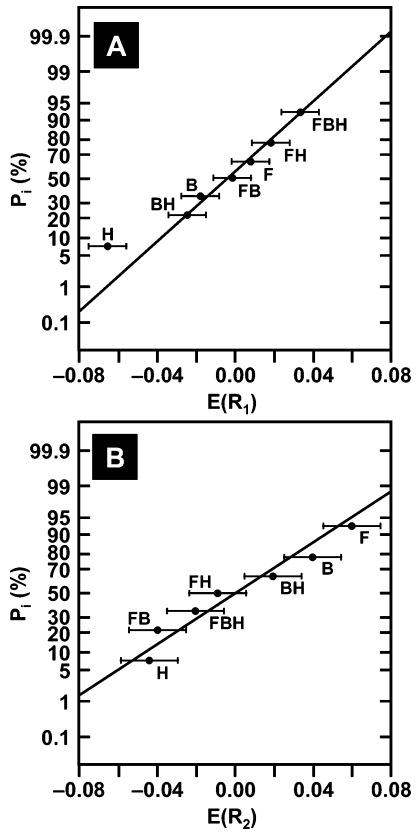

Figure 4. Normal probability plot analyses. (A) Analysis of the Fe plating mass effects, $E(R_1)$. The plot of P_i, calculated from eq 1, vs $E(R_1)_i$ is shown. The corresponding residuals plot of the [$\Delta(R_1)_i$, P_i] pairs, calculated from eq 2, is shown as Figure S1 in the Supporting Information. Numerical values for the [$E(R_1)_i$, P_i] and [$\Delta(R_1)_i$, P_i] pairs are listed in Supporting Information Tables S1 and S2, respectively. (B) Analysis of the percentage of plated fibers effects, $E(R_2)$. The plot of P_i, calculated from eq 1, vs $E(R_2)_i$ is shown. Because no variable or combination of variables influenced $E(R_2)$, no residuals plot is shown. Numerical values for the [$E(R_2)_i$, P_i] pairs are listed in Supporting Information Table S3. For all plots, variables or combinations of variables associated with each effect point are identified by the code letters as defined in Table 1.

percentage of metal-plated fibers (R_2) is not affected by any of the variables or combinations thereof over the ranges studied in matrix II. Consequently, our plating process exhibits wide process latitude and is well described by a simple model in which bath pH is the primary factor influencing metal deposition.

To better understand and characterize the nature of the plate, we randomly selected the sample from experiment 8 of matrix II for more detailed study. Neutron activation analysis of the plated fibers confirmed the presence of large amounts of Fe (30.9 ± 1.3 wt %) from the plate and traces of Pd (0.110 ± 0.004 wt %) and Sn (0.191 ± 0.006 wt %) from the catalyzed fiber, as expected. Further analysis indicated that small amounts of boron (1.99 ± 0.10 wt %) were also present in the sample. Normally, the identification of boron in an electroless Fe metal sample would suggest the presence of Fe−B alloy(s).[6,8,11,12] In this case, however, our use of borate buffer represents a possible alternative boron source, since borate is known to bind vicinal diols such as those present in the sugar residues of cellulose fibers.[37] Adsorption of borate to the surface of iron and/or its oxides during iron surface passivation has also been

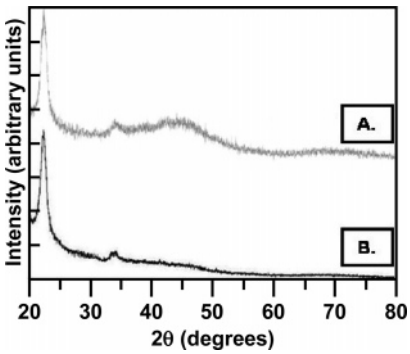

Figure 5. XRD spectra of the fibers: (A) Fe-plated fibers from sample 8 of matrix II, (B) raw cellulose fibers (control).

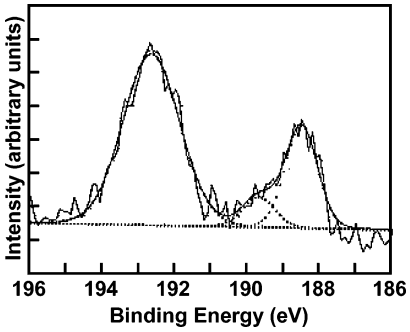

Figure 6. XPS B(1s) spectrum. Spectrum and peak deconvolution is shown for sample 8 of matrix II.

demonstrated,[38] providing yet another potential boron source that must be considered.

XRD and XPS analyses provide additional information concerning boron in our system. The XRD spectrum in Figure 5 for sample 8 (curve A) exhibits diffraction peaks at 22° (strong, sharp) and 34° (moderate, moderate) clearly identified with the cellulose fiber control (curve B), as well as at 45° (moderate, broad) and ~65−70° (weak, very broad) from the plate. Although the low intensity and corresponding positional uncertainty preclude definitive identification of the peak at ~65−70°, the 45° peak is tentatively assigned as Fe (bcc, 110). From the width (i.e., fwhm) of the 45° peak and using Scherrer's equation, we calculate a crystallite particle size of $\leq 0.7 \pm 0.2$ nm, consistent with a plate comprising an essentially amorphous Fe phase.

The presence of boron alloyed with this Fe phase is confirmed by the XPS B(1s) spectrum in Figure 6. A strong peak comprising ~70% of the total signal area observed at 192.7 eV signifies the presence of borate.[39] However, the remaining signal in the energy range 187.5 eV−190.5 eV is consistent with the presence of Fe−B alloy(s).[39] Although the asymmetry of this band (additional intensity at higher energy) suggests the presence of at least two alloy components at 188.5 eV (major, ~77%) and 189.7 eV (minor, ~23%), we lack sufficient information to determine the composition and percentage of each alloy at this time.[34] Therefore, we report an average alloy composition of $Fe_{10\pm1}B$ estimated from the neutron activation analysis data for Fe and B and the fraction of boron present as alloy from Figure 6.

Conclusions

In summary, we have employed two-level factorial statistical design methods to develop a new electroless Fe bath capable of functioning at room temperature without the need for an accompanying galvanic couple. The bath utilizes Fe(II) (0.025−0.050 M) complexed by citrate ligand (0.125−0.250 M) as a metal source in alkaline solution, with borate buffer (0.250 M total borate, pH 9.7−10.2) as a pH controller and borohydride (0.025−0.100 M) as the reductant. Statistical investigations of these variables over the ranges indicated show that only bath pH affects the quantity of metal deposited, with somewhat larger amounts of metal plated at lower pH. Plating of Pd/Sn-catalyzed cellulose microfibers is essentially complete (>98%) and is not influenced by any of the variables under these conditions, providing a wide process window for metal deposition. Surface analysis following plating confirms the deposition of an adherent amorphous ferromagnetic FeB coating of estimated thickness ~140−346 nm and composition ~$Fe_{10}B$ onto the microfiber surface. Work is continuing to further extend the ranges of the variables and explore temperature effects for our plating process, as well as characterize the physical and chemical properties of the plated metal and electromagnetic properties of composites containing the iron-plated cellulose fibers.[34]

Acknowledgment. We are grateful to the U.S. Naval Research Laboratory for financial support for this work through the NRL base 6.2 core funding program. C.N.K. thanks the National Research Council for financial support through an NRC postdoctoral fellowship.

Supporting Information Available: Description of the factorial analysis method, tables of analysis algorithm matrix data, and plot of residuals for some of that data (PDF). This material is available free of charge via the Internet at http://pubs.acs.org.

CM060649O

(37) (a) Rietjens, M.; Steenbergen, P. A. *Eur. J. Inorg. Chem.* **2005**, No. 6, 1162. (b) Kim, S. H.; Hyun, K.; Moon, T. S.; Mitusmata, T.; Hong, J. S.; Ahn, K. H.; Lee, S. J. *Polymer* **2005**, *46*, 7156. (c) Todorov, T. I.; Yamaguchi, Y.; Morris, M. D. *Anal. Chem.* **2003**, *75*, 1837. (d) Shao, C.; Miyazaki, Y.; Matsuoka, S.; Yoshimura, K.; Sakashita, H. *Macromolecules* **2000**, *33*, 19.

(38) Martini, E. M. A.; Muller, I. L. *J. Braz. Chem. Soc.* **1999**, *10*, 505.

(39) Moulder, J. F.; Stickle, W. F.; Sobol, P. E.; Bomben, K. D. In *Handbook of X-ray Photoelectron Spectroscopy*; Chastain, J., King, R. C., Jr., Eds.; Physical Electronics Inc.: Eden Prairie, MN, 1995; p 36.